Electronic Supplementary Information (ESI)

In situ atomic-resolution imaging of structural evolution and size-dependent melting point suppression in gold nanoclusters‡

Shengyong Hu,[†a,b] Kuo-Juei Hu,[†a,b,*] Zixiang Zhao[a,b]; Yongxin Zhang[a,b]; Syed Adil Shah[c];

Siqi Lu[a,b]; Wuwen Zhu[a,b]; Sichen Tang[a,b]; Fengqi Song [a,b,*]

[a]National Laboratory of Solid State Microstructures, Collaborative Innovation Center of Advanced Microstructures, School of Physics, Nanjing University, Nanjing 210093, China

[b]Institute of Atom Manufacturing Suzhou Campus, Department, Nanjing University, Nanjing 215163, China

[c]School of Biomedical Engineering, Health Science Centre, Shenzhen University Shenzhen, Guangdong 518060, PR China

[†]These authors contributed equally to this work

‡Electronic supplementary information (ESI) available

[*]Corresponding authors: kuojueihu@nju.edu.cn (Kuo-Juei Hu); songfengqi@nju.edu.cn (Fengqi Song)

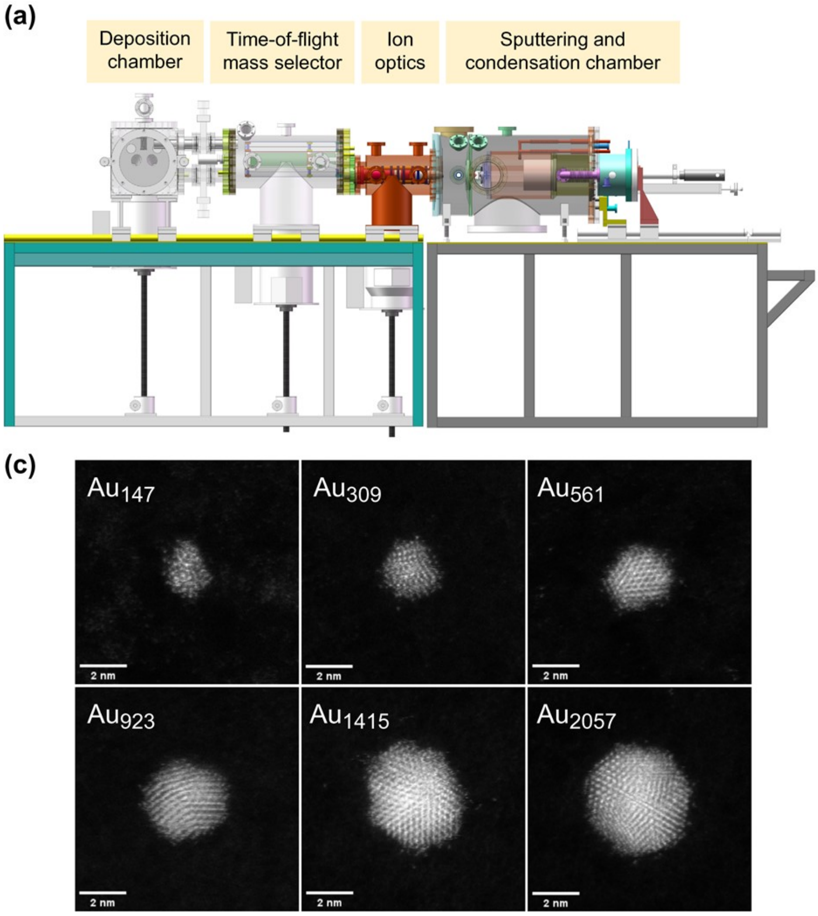

Figure S1. (a) Schematic of the cluster beam source that is combined with a magnetron sputtering and gas-phase condensation chamber, ion optics, a time-of-flight mass selector, and a deposition chamber. (b) Mass spectra of the gold clusters. (c) High-resolution HAADF-STEM images of the Au_N clusters (N = 147, 309, 561, 923, 1415, and 2057). (d) Integrated HAADF intensities of the Au_N clusters as a function of the corresponding of cluster size (N = 147, 309, 561, 923, 1415, and 2057).

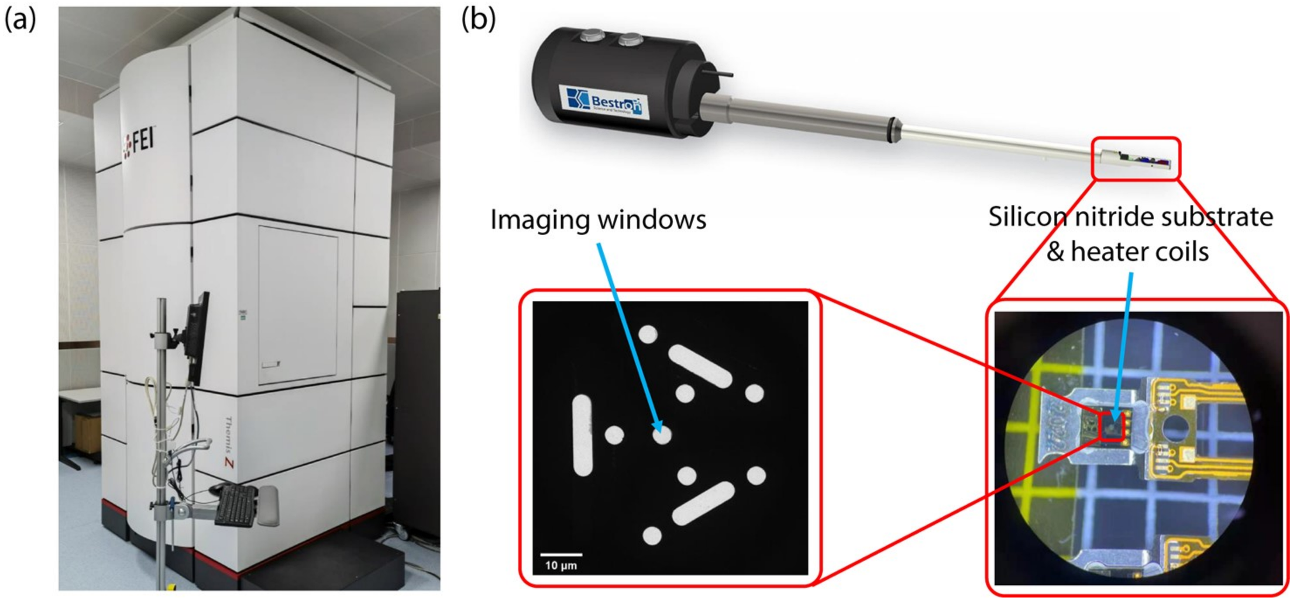

Figure S2. (a) Aberration-corrected scanning transmission electron microscope (200 kV FEI Themis Z) at the National Graphene Products Quality Inspection and Testing Center in Wuxi, China. (b) Double-tilt in situ heating holder coupled with in situ heating chip.

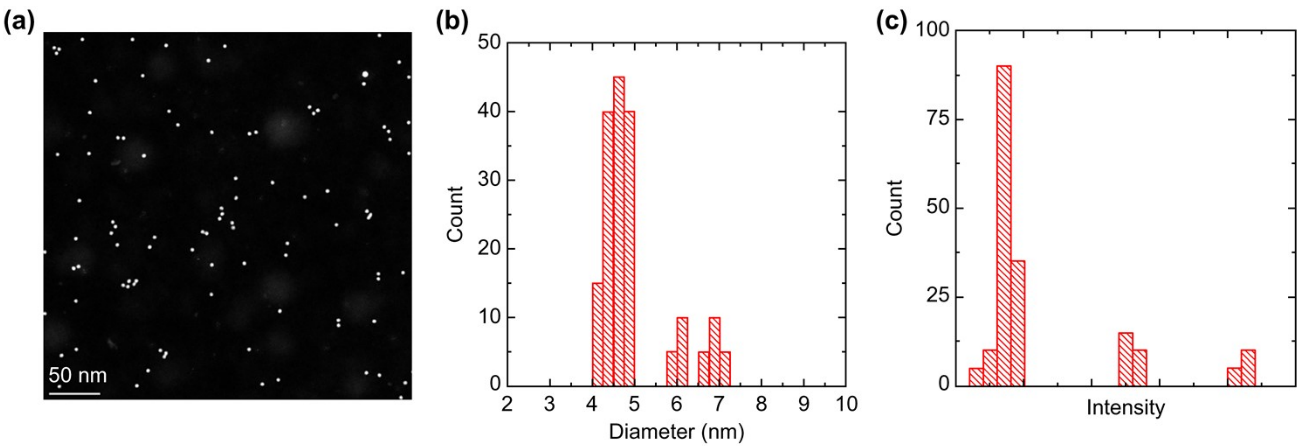

Figure S3. (a) HAADF-STEM image of the Au_{2057} clusters. The corresponding size distribution and HAADF intensity statistics are depicted in parts (b) and (c), respectively.

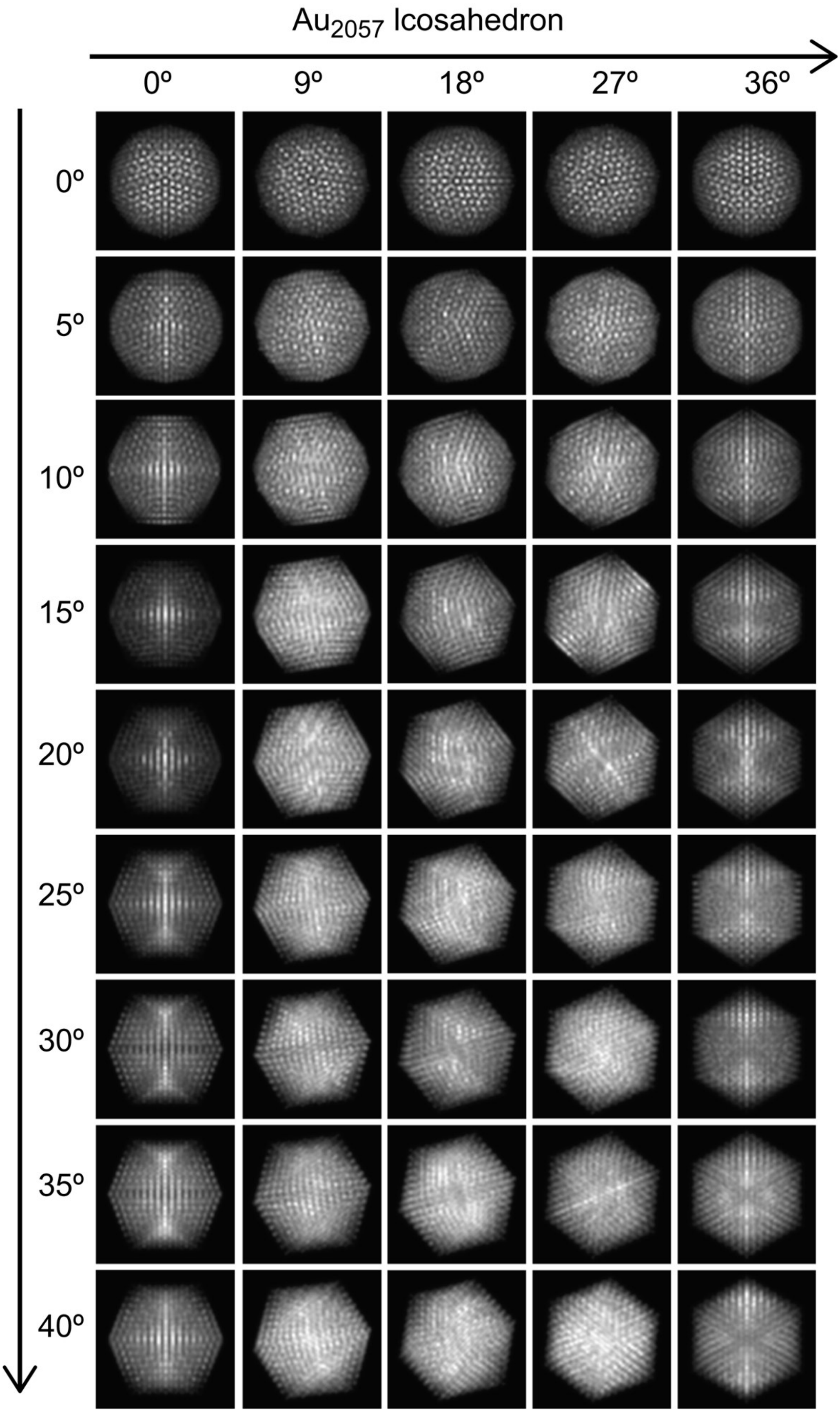

Figure S4. QSTEM simulated atlas of the Au_{2057} icosahedron (Ih).

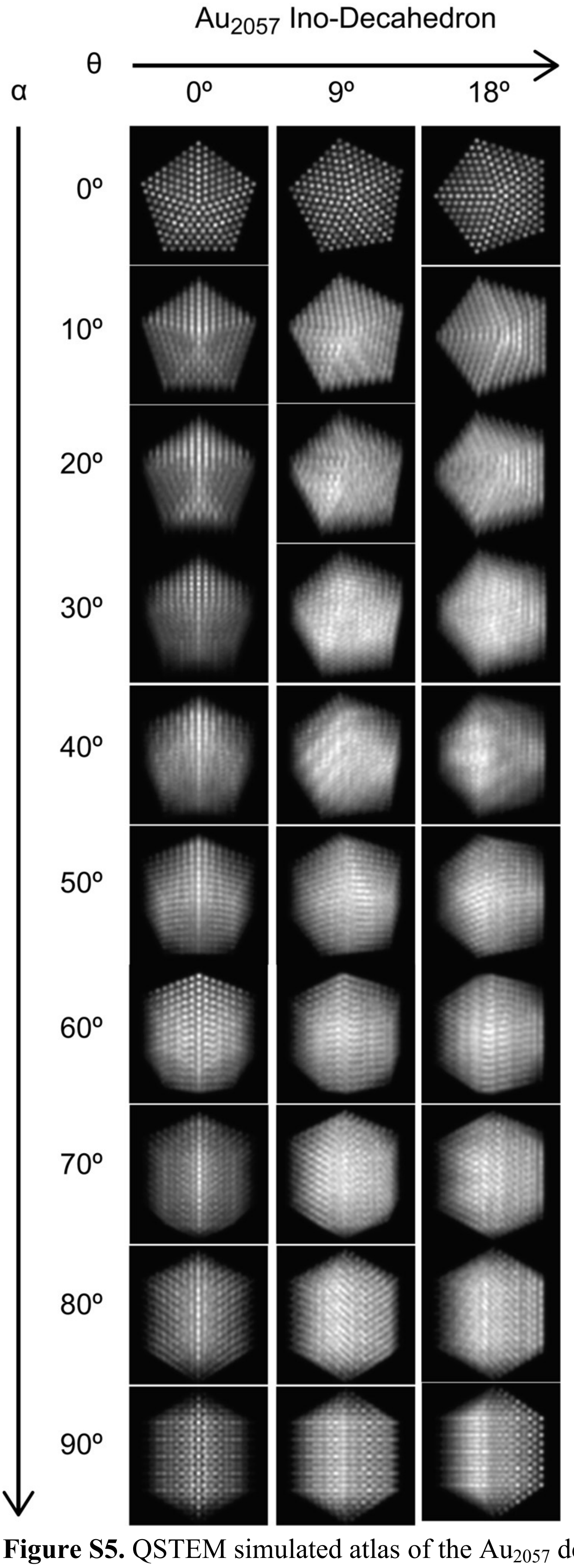

Figure S5. QSTEM simulated atlas of the Au_{2057} decahedron (Dh)

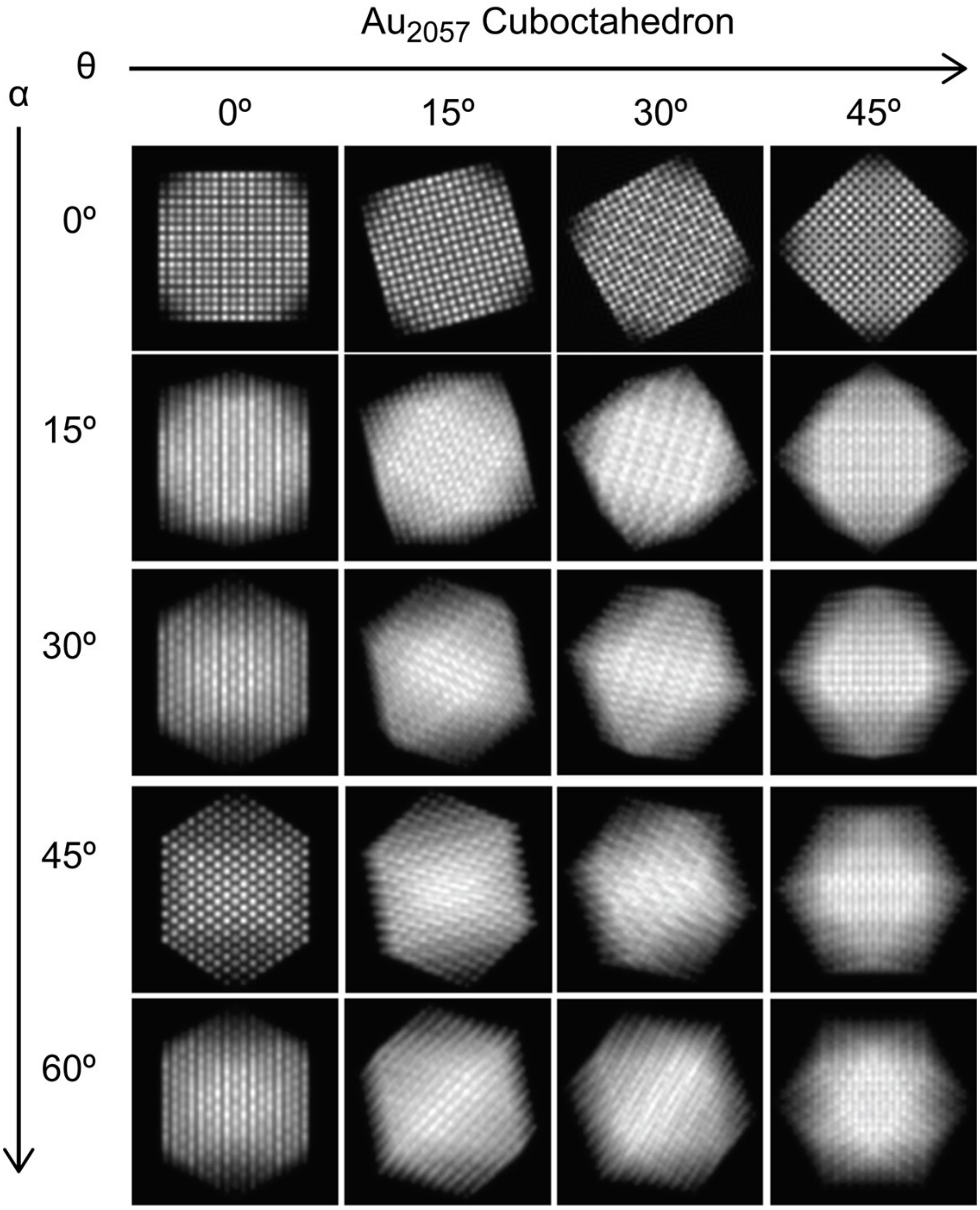

Figure S6. QSTEM simulated atlas of the Au_{2057} face-centered cubic (FCC) structure.

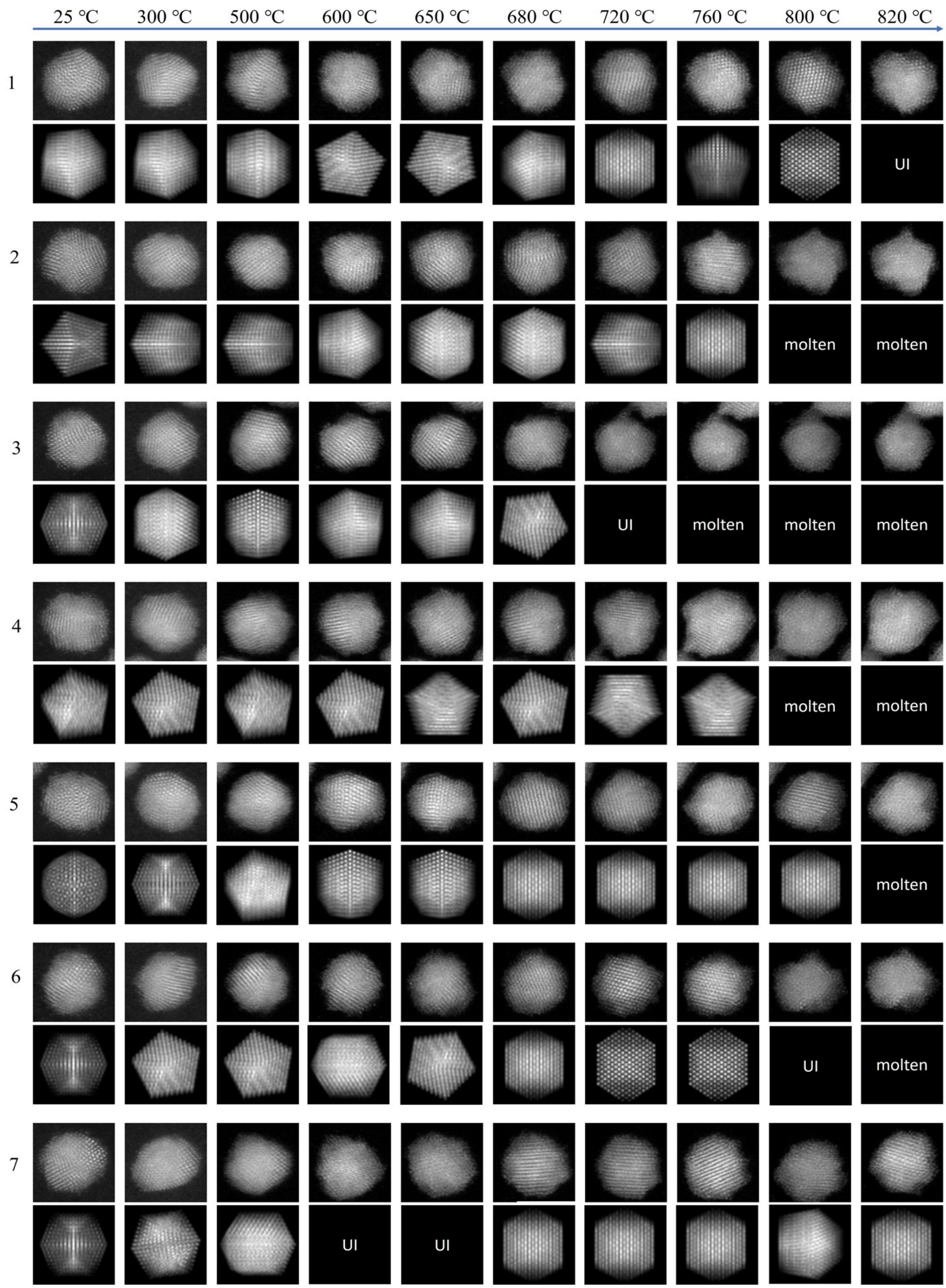

Figure S7. Representative HAADF-STEM images of the Au_{2057} clusters and the corresponding QSTEM multi-slice image simulations at each temperature.

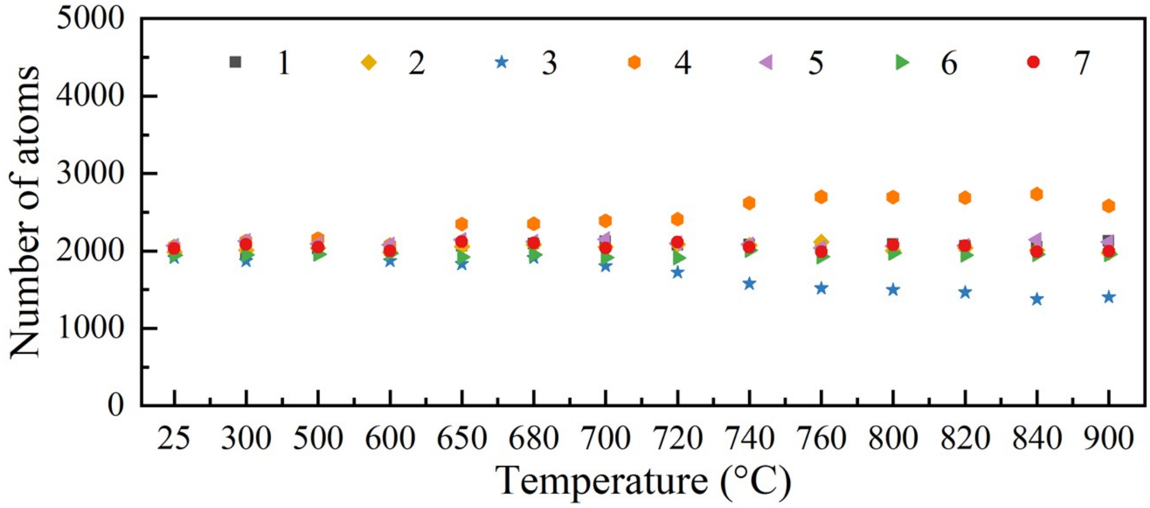

Figure S8. Variation in the atom counts of the $Au_{2057\pm51}$ clusters versus the temperature during the in-situ heating process.

Melting models

Pawlow's Model:[1,2]

$$T_m = T_0\left(1 - \frac{2V_s}{rH_m}\left(\sigma_s - \sigma_l\left(\frac{\rho_s}{\rho_l}\right)^{2/3}\right)\right)$$

Thomson's model:[3,4]

$$T_m = T_0\left(1 - \frac{2(\sigma_s - \sigma_l)V_s}{rH_m}\right)$$

The liquid shell model:[5–8]

$$T_m = T_0\left(1 - \frac{2V_s}{H_m}\left(\frac{\sigma_s - \sigma_l}{r - t} + \frac{\sigma_l}{r}\left(1 - \left(\frac{\rho_s}{\rho_l}\right)^{2/3}\right)\right)\right)$$

The lower boundary of the LNG model:[9]

$$T_{m-lb} = T_0\left(1 - \frac{3(\sigma_s - \sigma_l)V_x}{rH_m}\right)$$

The upper limit is given by the Gibbs- Thomson equation:[9]

$$T_{m-ub} = T_0\left(1 - \frac{2(\sigma_s - \sigma_l)V_s}{rH_m}\right)$$

The critical radius in the LNG model is given by:[9]

$$r_c = \frac{2(\sigma_s - \sigma_l)V_sT_0}{H_m(T_0 - T)}$$

Table S1. Constants used for plotting the melting models in Figure 6

Symbol	Meaning	Value	Unit	Reference
T_0	Bulk melting temperature	1064.18	°C	10,11
V_s	Molar volume of the solid	1.021×10^{-5}	m^3/mol	12
H_m	Molar latent heat	12552	J/mol	10,11
σ_s	Surface tension of the solid	1.4	J/m^2	13,14
σ_l	Surface tension of the liquid	1.135	J/m^2	13,14
ρ_s	Mass density of the solid	19300	kg/m^3	12
ρ_l	Mass density of the liquid	17310	kg/m^3	12

References

1 A. Barybin and V. Shapovalov, Modification of Pawlow's thermodynamical model for the melting of small single-component particles, *Journal of Applied Physics*, 2011, **109**. DOI: 10.1063/1.3544468.

2 P. Pawlow, The dependency of the melting point on the surface energy of a solid body, *Z. phys. Chem*, 1909, **65**, 545–548.

3 J. J. Thomson, *Applications of dynamics to physics and chemistry*, Macmillan, 1888.

4 G. Kaptay, The Gibbs equation versus the Kelvin and the Gibbs-Thomson equations to describe nucleation and equilibrium of nano-materials, *Journal of nanoscience and nanotechnology*, 2012, **12**, 2625–2633.

5 H. REISS and I. B. WILSON, The effect of surface on melting point, *Journal of colloid science*, 1948, **3**, 551–561.

6 N. D. Lisgarten, J. R. Sambles and L. M. Skinner, Vapour pressure over curved surfaces-the Kelvin equation, *Contemporary Physics*, 1971, **12**, 575–593.

7 R. Kofman, P. Cheyssac, A. Aouaj, Y. Lereah, G. Deutscher, T. Ben-David, J. M. Penisson and A. Bourret, Surface melting enhanced by curvature effects, *Surface Science*, 1994, **303**, 231–246.

8 K.-J. Hanszen, Theoretische Untersuchungen ber den Schmelzpunkt kleiner Kgelchen, *Z. Physik*, 1960, **157**, 523–553.

9 P. R. Couchman and W. A. Jesser, Thermodynamic theory of size dependence of melting temperature in metals, *Nature*, 1977, **269**, 481–483.
10 Collaboration: Scientific Group Thermodata Europe (SGTE), Thermodynamic Properties of Elements, Ac to C60, *Pure Substances. Part 1 _ Elements and Compounds from AgBr to Ba3N2*, 1999, 1–24.
11 G. Guenther and O. Guillon, Models of size-dependent nanoparticle melting tested on gold, *J Mater Sci*, 2014, **49**, 7915–7932.
12 Technical data for the element Gold in the Periodic Table, https://periodictable.com/Elements/079/data.html, (accessed 25 April 2024).
13 P. Buffat and J.-P. Borel, Size effect on the melting temperature of gold particles, *Phys. Rev. A*, 1976, **13**, 2287–2298.
14 J. R. Sambles, An electron microscope study of evaporating gold particles: the Kelvin equation for liquid gold and the lowering of the melting point of solid gold particles, *Proc. R. Soc. Lond. A*, 1971, **324**, 339–351.